



A new approach for rapid electrolyte wetting in tape cast electrodes for lithium-ion batteries

Journal:	<i>Journal of Materials Chemistry A</i>
Manuscript ID:	TA-ART-05-2014-002353.R2
Article Type:	Paper
Date Submitted by the Author:	25-Jul-2014
Complete List of Authors:	Pfleging, Wilhelm; Karlsruhe Institute of Technology, Institute for Applied Materials (IAM-AWP) Pröll, Johannes; Karlsruhe Institute of Technology, Institute for Applied Materials (IAM-AWP)

PAPER

A new approach for rapid electrolyte wetting in tape cast electrodes for lithium-ion batteries

Cite this: DOI: 10.1039/x0xx00000x

Wilhelm Pfleging^{a,b} and Johannes Pröll^aReceived 00th January 2012,
Accepted 00th January 2012

DOI: 10.1039/x0xx00000x

www.rsc.org/

An innovative concept for significantly decreasing the time-span for the electrochemical formation step after lithium-ion cell assembly is presented. Laser structuring has been developed for the formation of capillary microstructures in tape cast electrodes resulting in a tremendous acceleration of electrolyte wetting in comparison to unstructured electrodes. Pouch cells with laser-structured electrodes show an increase in capacity retention and an enhancement in cell cycle life-time at high charging and discharging rates. We assume that laser structuring of tape cast electrodes could be a further step towards economic and zero failure production of high-power lithium-ion batteries.

Introduction

Within the last two decades lithium-ion batteries have emerged as the power source of choice for the high performance rechargeable battery market.^{1, 2} The development of three dimensional (3D) surface structures in electrodes for lithium-ion cells is a very promising approach in order to counter effects which can lead to reduced electrochemical performance, e.g. one dimensional lithium-diffusion, poor capacity retention at high charging/discharging currents, high ohmic resistance³ or mechanically induced tension in the active material⁴ due to lithiation and delithiation processes.

3D electrode architectures enable large areal energy densities due to an increased active surface^{3, 5, 6} which are of interest especially for thin-film batteries since lithium-ion diffusion within the compact thin-film electrodes is limited by their thickness.

A common approach for realisation of 3D architectures in electrodes is the structuring of the substrate or current collector, e.g. via template deposition of nanorods or via anisotropic etching of silicon.⁵⁻⁷ These technical approaches are applied for thin-film batteries but may be not feasible for thick-film electrodes.^{3, 8-12}

A rather new technical approach is laser structuring of the active material itself for realisation of 3D architectures which

has been realised for thin film electrodes made of LiCoO₂, LiMn₂O₄, SnO₂ or fluorine doped SnO₂.^{4, 13-21} For each type of electrode material a significant improvement of specific capacity and cycle retention at high charging/discharging has been achieved due to laser patterning and laser annealing. Within a recent approach it has been shown that laser patterning processes can also be applied for LiCoO₂ and LiMn₂O₄ composite electrodes with film thicknesses of up to 100 μm.²²⁻²⁴ Lithium-ion cells with laser-structured cathodes exhibit improved capacity retention, higher specific capacities at higher charging and discharging currents compared to lithium-ion cells with unstructured cathode films.

A main objective of current research is to transfer the laser technology for structuring of thin-film and thick-film electrode materials from laboratory scale to large areal tape cast electrodes being more relevant for industrial production of lithium-ion batteries (LIB) for stationary²⁵ and portable²⁶ power systems as well as for the development of cost efficient full electrical vehicles. State-of-the-art batteries with pouch cell geometry for high-power applications consist of up to 100 layers made of anode sheets, separator membranes and cathode sheets which are stacked for achieving capacities of up to 40-50 Ah. The electrode materials with typical film thicknesses of 20-100 μm are deposited, e.g. by tape casting on 10-20 μm thick aluminium (cathode) or copper (anode) current collectors. After stacking of the anodes, separators and cathodes, each of these layers must be wetted homogenously with liquid electrolyte. Generally, electrolyte filling of pouch cells is realised by time and cost consuming vacuum and storage processes at elevated temperatures. Nevertheless, by applying current electrolyte filling processes insufficient wetting of

^a Karlsruhe Institute of Technology (IAM-AWP), Germany, E-mail: wilhelm.pfleging@kit.edu, johannes.proell@kit.edu

^b Karlsruhe Nano Micro Facility (KNMF), Karlsruhe, Germany

† Electronic Supplementary Information (ESI) available. See DOI: 10.1039/b000000x/

electrode surfaces is one drawback resulting in a certain production failure rate, a lowered cell capacity or a reduced battery life-time.

In this work we present a novel and cost efficient laser-based technology for the realisation of 3D architectures in thick-film tape cast electrodes for enabling a fast and homogeneous wetting of electrodes with liquid electrolyte as well as a stable electrochemical cell operation.

Experimental

Electrode Materials

The used electrode material consists of active material lithium nickel manganese cobalt oxide ($\text{Li}(\text{NiMnCo})\text{O}_2$), carbon black, graphite and binder. In the following, this composite material will be denoted as NMC. Due to confidential agreement of KIT with the NMC material supplier, the latter does not want to receive any consideration in this text.

NMC thick films were used for laser structuring experiments, for measurements of the capillary rise of liquid electrolyte as well as for assembling lithium-ion cells for long-term cycling. The films had a thickness of about $(55 \pm 2) \mu\text{m}$ and were coated onto $20 \mu\text{m}$ thick aluminium current collectors (Figure 1). The NMC material was analysed by inductively coupled plasma optical emission spectrometry (ICP-OES). The resulting elemental mass weights were as follows: Li: $5.50 \text{ wt.}\% \pm 0.01 \text{ wt.}\%$; Mn: $14.39 \text{ wt.}\% \pm 0.08 \text{ wt.}\%$, Ni: $15.14 \text{ wt.}\% \pm 0.02 \text{ wt.}\%$ and Co: $15.44 \text{ wt.}\% \pm 0.23 \text{ wt.}\%$. The lithium to transition metal ratio was calculated to be $n_{\text{Li}}/n_{\text{M}} = 1.01$ where $M = \text{Ni} + \text{Co} + \text{Mn}$.

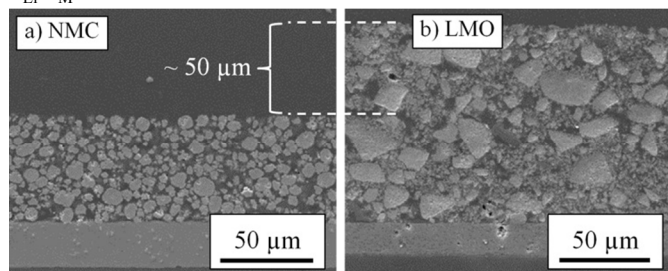


Figure 1: Cross-sectional SEM images of (a) $55 \mu\text{m}$ thick NMC and (b) $103 \mu\text{m}$ thick LMO film.

As anode material, $55 \mu\text{m}$ thick graphite layers tape-casted onto $10 \mu\text{m}$ thick copper foil were used. The separator membranes consisted of a polyethylene film with an averaged thickness of $21 \mu\text{m}$ (MTI Corporation, USA). Polyethylene films are widely used as separators in lithium-ion cells but are known to exhibit quite poor electrolyte wetting behaviour compared to modified polymeric base materials²⁷ and are therefore, suitable for investigations for improving the electrolyte wetting for commercially available materials.

In order to carry out comparative studies, selected electrolyte wetting experiments were investigated using cathodes from MTI Corporation (USA) with lithium manganese oxide (LiMn_2O_4) as active material. In the following, this composite material will be denoted as LMO. The active material proportion was $94.5 \text{ wt.}\%$ while $5.5 \text{ wt.}\%$ were

assigned to PVDF binder, carbon black and graphite. The LMO film thickness was measured to $(103 \pm 1) \mu\text{m}$ (Figure 1). Through ICP-OES analysis a lithium to manganese ratio of $n_{\text{Li}}/n_{\text{Mn}} = 0.55$ (Li: $3.22 \text{ wt.}\% \pm 0.02 \text{ wt.}\%$; Mn: $46.70 \text{ wt.}\% \pm 0.03 \text{ wt.}\%$) could be determined.

Laser-assisted structuring of electrode materials

Laser patterning was performed using a Q-switched Yb fiber laser (Type: YLP-1/100/20, IPG Photonics Corporation, USA) operating at a wavelength of $\lambda = 1064 \text{ nm}$ with a tunable pulse repetition rate in the range of $20 - 80 \text{ kHz}$ (Table 1). The laser pulse duration was measured to 200 ns (FWHM). The laser radiation source was implemented in a laser workstation PIRANHA from ACSYS Lasertechnik GmbH (Kornwestheim, Germany). The laser beam was scanned over the sample surface by deflection mirrors with scanning velocities in the range of 100 mm/s to 1800 mm/s . The laser focus diameter was $23 \mu\text{m}$. All experiments were carried out under ambient air and the ablated material was removed by an exhaust.

Table 1 Laser structuring parameters

Wavelength [nm]	Pulse duration [ns]	Pulse repetition rate [kHz]	Average laser power [W]	Laser scan velocity [mm/s]
1060 - 1070	200	20 - 80	5 - 16	100 - 1800

Characterization of surface and wetting properties

The morphologies of the as-received electrodes as well as the geometries of laser-induced channel structures were investigated by scanning electron microscopy (Philips XL 30S and Jeol 840 Scanning Microscope). The ablation depths and surface topographies were measured by white light profilometry using the MicroProf[®] white light profilometer from Fries Research & Technology GmbH (Bergisch Gladbach, Germany). The wetting properties prior to as well as after laser modification were examined by measuring the maximum capillary rise height h_{max} of the electrolyte within unstructured and laser-structured electrodes (Figure 2).

For this kind of experimental set-up, a vertical arrangement (Figure 2) was chosen in order to examine the most efficient microstructure geometry enabling homogeneous wetting even versus gravity. In the pouch cell assembly process, the liquid electrolyte is generally injected in a vertical arrangement into the pre-assembled electrode stack prior to vacuuming and final sealing while a considerable amount of liquid electrolyte piles up at the bottom of the electrode stack after the first electrolyte injection. For this purpose, unstructured and laser-structured cathodes with outer dimensions of $20 \cdot 65 \text{ mm}^2$ were established. The bottom part of each sample was dipped into the liquid (DMC, LP 30) in a way that the electrodes were completely immersed in the liquid over a height of about 5 mm (Figure 2).

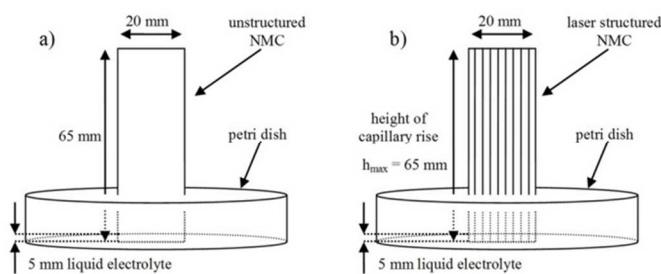


Figure 2: Schematic of the experimental set-up for investigation of the capillary rise in (a) unstructured and (b) laser-structured electrodes.

Pouch cells and electrochemical tests

Pouch cell manufacturing was performed in an argon-filled glove box of type LABmaster sp (MBraun Inertgas-Systeme GmbH, $H_2O < 0.1$ ppm, $O_2 < 0.1$ ppm). Each pouch cell consisted of one anode, one separator layer and one cathode. The outer electrode dimensions were 50×50 mm² for each cathode layer, 54×54 mm² for each anode layer and 58×58 mm² for each of the separator membranes.

The liquid electrolyte was composed of ethylene carbonate and dimethyl carbonate mixed in a 1:1 ratio including one molar lithium hexafluorophosphate salt (EC/DMC 1:1, 1M LiPF₆, LP 30, Merck AG, Germany). An equal amount of liquid electrolyte was filled between each, the cathode/separator interface as well as the anode/separator interface by using a pipette. The electrolyte was filled into the layers in a way that the filling direction and the laser-generated capillary structures were aligned. The manufacturing steps were equal for both, assembling cells with unstructured or laser-structured electrodes.

Lithium-ion pouch cells were electrochemically cycled using a battery cycler of type BT2000 (Arbin Instruments, USA). Electrochemical priming of all lithium-ion cells was carried out for three cycles in a voltage window ranging from 3.0 V to 4.2 V. Lithium-ion cells stored for 24 hours after the assembly process were electrochemically primed using the constant current constant voltage method: Once the upper cut-off voltage of 4.2 V was reached, the cell voltage was stabilised until the current dropped below a C/20 value, referring to the charging current. Within the third formation cycle, the lithium-ion cells were discharged to 3.7 V. The charging and discharging rates were C/10 for the first charge and C/2 for the following half-cycles.

The formation procedure for lithium-ion cells electrochemically cycled without 24 hours storage was carried out for three cycles using a C/10 rate for both charge and discharge. After the priming procedure, long-term cycling for all lithium-ion cells was carried out at a 1 C charging and a 1 C discharging rate within a voltage window of 3.0 V to 4.2 V and cycles numbers of up to 3000. The C-rates were calculated using a capacity of $1.75 \text{ mAh} \cdot \text{cm}^{-2}$. The film mass of electrodes with a geometry of 50×50 mm² could be determined to (335 ± 2) mg. The film mass was reduced to (236 ± 4) mg after

laser structuring of NMC and therefore, formation of channel structures.

Results and Discussion

Formation of capillary structures in electrode materials

The laser beam energy is absorbed at the material surface. Due to heat conduction the temperature of the surrounding composite material increases. PVDF has a low decomposition temperature in the range of 250 - 350 °C.²⁸ Therefore, the PVDF binder matrix spontaneously evaporates and active particles are removed from the laser beam interaction zone. A similar ablation process for metal/polymer composite materials has already been described by Slocombe.²⁹ For a laser ablation process the ablation depth d [m] can be described as a function of laser power P_L [W] and laser scan velocity v [m/s] of the laser beam:^{30, 31}

$$d \propto \frac{P_L}{v} \quad (1)$$

Depending on the laser power and the laser scan velocity, the energy input and therefore, the ablation depth d varies. $L = P_L / v$ [J/m] is the so-called line energy.

Laser ablation of NMC thick-films was studied under ambient air for different line energies L (Figure 3).

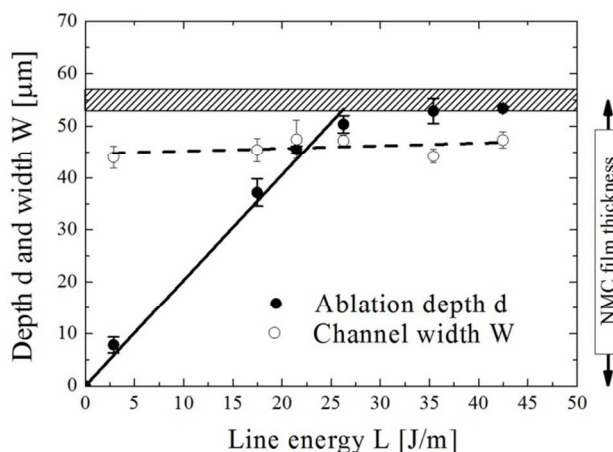


Figure 3: Laser ablation depth d and channel width W of NMC electrodes as function of line energy L (repetition rate $v_{\text{rep}} = 80$ kHz, laser scan velocity $v = 200$ mm/s, processing gas: ambient air).

For this purpose, the laser repetition rate v_{rep} as well as the laser scan velocity rate v were kept constant ($v_{\text{rep}} = 80$ kHz, $v = 200$ mm/s). The ablation depth d linearly increases as function of line energy up to $L = 26$ J/m. This is in good agreement with equation (1). For larger line energies L , the ablation depth d reaches its maximum limited by the composite film thickness of (55 ± 2) μm as indicated in Figure 3. The channel width W possesses a nearly constant behaviour for all considered line energies and reaches values of 44 - 47 μm. In order to completely remove the NMC film from the laser ablation interaction zone, appropriate laser parameters were

investigated resulting in a line energy of $L = 42.5 \text{ J/m}$ (Figure 4a). This line energy corresponds to an average laser power of $P = 8.5 \text{ W}$, a laser scan velocity of 200 mm/s and a laser repetition rate of $\nu_{\text{rep}} = 80 \text{ kHz}$. By using these parameters, an array of line grooves with a pitch distance of $200 \mu\text{m}$ (Figure 4b) could be realised for both geometries, $20\text{-}65 \text{ mm}^2$ (single-side coated wetting samples) and $50\text{-}50 \text{ mm}^2$ (single-side coated pouch cell samples). Figure 4b demonstrates that laser structuring can be realised even for double-side coated aluminum substrates which is a required processing step for process up-scale for manufacturing of lithium-ion cells with high capacities.

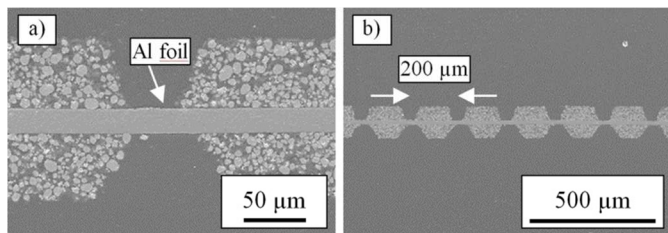


Figure 4: SEM images of laser-structured NMC thick films in cross-sectional view; overview (a) and detail view (b); laser parameters for structuring: average laser power $P = 8.5 \text{ W}$, repetition rate $\nu_{\text{rep}} = 80 \text{ kHz}$, laser scan velocity $v = 200 \text{ mm/s}$, laser pitch distance: $200 \mu\text{m}$.

The patterning process was also studied using LMO thick films. Large area patterning (Figure 5a) of the $103 \mu\text{m}$ thick LMO coatings was possible using the same laser parameters resulting in a line energy of $L = 42.5 \text{ J/m}$. It could be shown that the NMC and LMO thick films could be completely removed within the laser treated area down to the aluminium substrate (Figure 5b). It is well-known that the particle size and the crystalline structure significantly influence the electrochemical performance of electrode materials. Through SEM and XRD measurements (not shown here) no changes in particle size and crystalline structure due to laser-treatment could be detected.

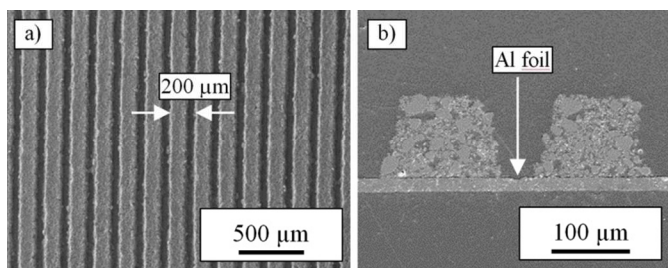


Figure 5: Top-view SEM image of laser-structured LMO thick film (a) and cross-sectional view (b); laser parameters for structuring: $P = 8.5 \text{ W}$, $\nu_{\text{rep}} = 80 \text{ kHz}$, $v = 200 \text{ mm/s}$, pitch distance $200 \mu\text{m}$.

Finally, the presented laser parameters were applied in a first step to generate wetting samples ($20\text{-}65 \text{ mm}^2$) and in a second step for large areal ($50\text{-}50 \text{ mm}^2$) laser structuring of single-side coated electrodes which were necessary for lithium-ion pouch cell assembly.

Influence of laser-induced capillary geometry on the wetting height

The wetting behaviour of unstructured and laser-structured electrodes was investigated using the experimental set-up described in Figure 2. In a first approach, the capillary rise as function of channel width W was investigated (Figure 6).

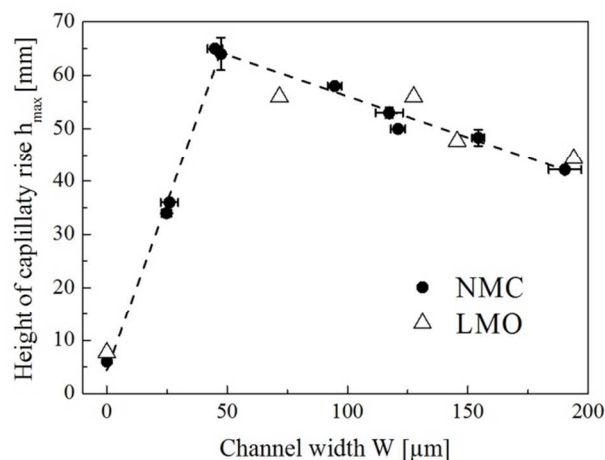


Figure 6: Maximum height of capillary rise of DMC and LP 30 in NMC and LMO thick films as function of laser-induced groove width.

Obviously, for a channel width of about $40\text{-}55 \mu\text{m}$, a maximum height h_{max} of about 65 mm could be achieved. By increasing the channel width, the height of the maximum capillary rise decreased. In addition to the investigations presented for NMC films, measurements on the wetting behaviour of LMO film were performed (Figure 6). The dependence of h_{max} as a function of channel width W is almost the same as observed for the NMC film. Besides the channel width W , the channel depth d is also a critical capillary geometry parameter with respect to an optimized liquid electrolyte transport within the thick-film electrodes. Therefore, the wetting behaviour as function of channel depth d was investigated in correspondence to the experimental set-up in Figure 2. For this purpose, a channel width of about $47 \mu\text{m}$ was selected. The maximum height h_{max} of capillary rise linearly increases with channel depth d (Figure 7). For the maximum in channel depth $d = d_{\text{max}}$, the height of capillary rise indicates a sharp increase. Therefore, the removal of the complete electrode material ($d = d_{\text{max}}$) from the ablation zone delivers the most efficient capillary transport. Laser-generated channels in electrode materials with channel widths of about $40\text{-}55 \mu\text{m}$ and channel depths of $d = d_{\text{max}}$ – which corresponds to the NMC film thickness – act as optimized capillaries for an efficient distribution of liquid electrolyte within a thick-film composite electrode.

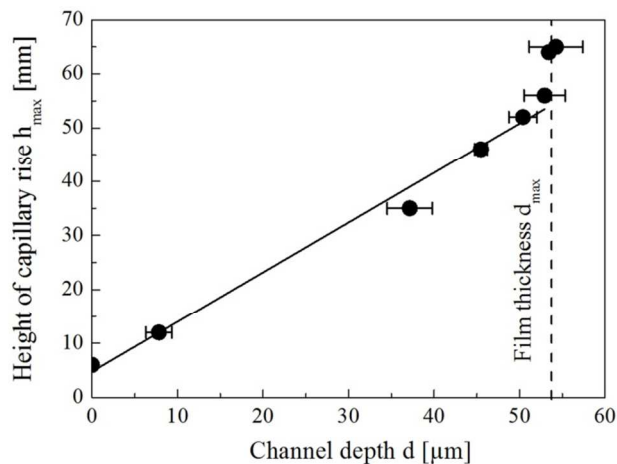


Figure 7: Maximum height of capillary rise of DMC in NMC films as function of channel depth (channel width 47 μm).

Another important issue related to the introduction of laser-based structuring technology in battery manufacturing is the time dependence of the liquid transport through the capillaries. For this reason, the presented results (Figure 6, Figure 7) obtained from the experimental set-up in Figure 2 will be discussed with respect to process transfer to large-area electrode geometry (50-50 mm^2) which was required for pouch cell assembly. Factors of influence such as vapourisation of the liquid or nano-sized porosity perpendicular to the capillary channel structures will be considered for discussion.

Time dependence of wetting in structured electrodes

The capillary rise h of liquids along the micro-channels can be described by the classical Washburn equation:^{32, 33}

$$\frac{dh}{dt} = \frac{r^2}{8\mu h} \left(\frac{2\sigma_l \cos\theta}{r} - \Delta\rho g h \right), \quad (2)$$

whereat h [m] is the height of capillary rise of the liquid within the capillary, t [s] is the capillary rise time, σ_l [kg/s^2] and μ [$\text{kg}/(\text{m}\cdot\text{s})$] are the surface tension and viscosity of the liquid, r [m] the capillary radius, $\Delta\rho$ [kg/m^3] the difference in density between liquid and the gas-phase, g [m/s^2] the acceleration due to gravity and θ [$^\circ$] the contact angle between the wall and the meniscus.

In case that gravity can be neglected and assuming that the capillary structure is filled at the beginning of the measurement ($t = 0$ s) up to an height of $h = h_0$, the integration of equation (2) delivers

$$h = h_0 + \sqrt{\frac{r\sigma_l \cos\theta}{2\mu}} \cdot t_h = h_0 + K \cdot t_h^{0.5} \quad (3)$$

whereat K [$\text{m}/\text{s}^{0.5}$] describes the penetration ability of the liquid and t_h [s] the capillary rise time for achieving the height h [m].³⁴

The time-dependence of the height of capillary rise was investigated for durations up to $t_h = 80$ s (Figure 8a). Figure 8b shows the corresponding experimental set-up (see Figure 2).

In comparison to the measured heights of the capillary rise of DMC in NMC films, additional measurements were

performed by using LP 30 and laser-structured LMO electrodes (Figure 8a). Regarding NMC films, the time dependence of the capillary rise can be divided into two parts. Up to a height of about $h = 50$ mm, a rapid wetting can be observed accompanied with a penetration ability of $K = 12 \text{ mm}/\text{s}^{0.5}$ (equation (3)). For wetting times $t_h > 12$ s, the penetration ability decreases to $K = 6 \text{ mm}/\text{s}^{0.5}$ (Figure 8a). Concerning the LMO film, the expected time dependence $h \sim t_h^{0.5}$ with respect to equation (3) could be reproduced very well for wetting times of up to $t_h = 80$ s, showing a penetration ability of $K = 6 \text{ mm}/\text{s}^{0.5}$ (Figure 8a).

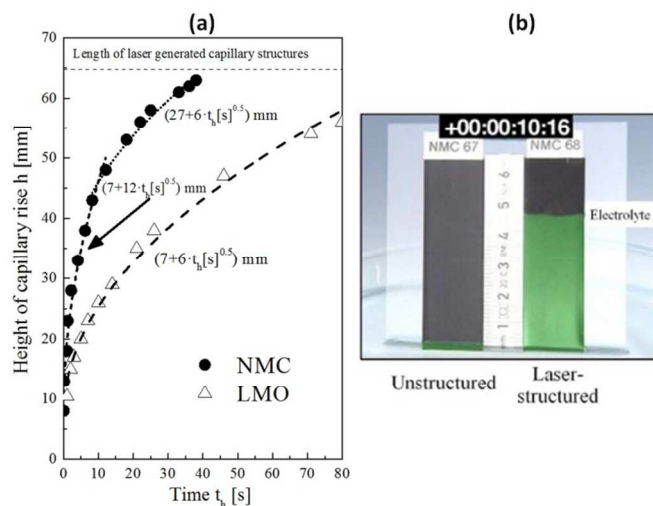


Figure 8: Height of capillary rise as function of time for laser-structured NMC (DMC, channel width 47 μm) and LMO (LP 30, channel width 70 μm) thick films and (b) snap-shot of video imaging the capillary rise h in dependence of wetting time t_h (~ 10 s).

The time dependence of the capillary rise as well as the penetration ability is mainly defined by the viscosity and surface tension. LP 30 is an organic electrolyte solution which consists of binary solvent systems such as a high permittivity solvent (ethylene carbonate, EC) mixed with a low viscosity alkyl carbonate (dimethyl carbonate, DMC) and LiPF_6 as the solute. In Table 2, the material properties of DMC and LP 30 with respect to density ρ , dynamic viscosity μ and surface tension σ_l are listed.

Table 2 Material properties of DMC and LP 30 for calculating the height h_{max} of capillary rise (equation (5))

DMC	LP 30 (EC/DMC 1:1, 1 M LiPF_6)
$\sigma_l(\text{DMC}) = 0.0288 \text{ kg}/\text{s}^2$ ³⁵	$\sigma_l(\text{EC/DMC, LiPF}_6) = 0.0303 \text{ kg}/\text{s}^2$ ³⁶
$\rho(\text{DMC}) = 1060 \text{ kg}/\text{m}^3$ ³⁷	$\rho(\text{LP 30}) = 1280 \text{ kg}/\text{m}^3$
$\mu(\text{DMC}) = 0.00063 \text{ Pa}\cdot\text{s}$ ³⁷	$\mu(\text{LP 30}) = 0.00338 \text{ Pa}\cdot\text{s}$ ³⁸

While the surface tension σ_l of DMC is almost similar to that of LP 30, the viscosities differ by a factor 5.4. With respect to

equation (3), it is expected that the capillary rise is suppressed by using LP 30 instead of DMC as wetting liquid, i.e. the penetration ability should decrease by a factor of $(5.4)^{0.5} = 2.3$ which is in good agreement with the experimental results shown in Figure 8: The wetting of NMC electrodes with DMC reveals a penetration ability of $K = 12 \text{ mm/s}^{0.5}$ (for $t_h < 12 \text{ s}$) while wetting of LMO with LP 30 delivers $K = 6 \text{ mm/s}^{0.5}$. Nevertheless, there is a change in penetration ability of laser modified NMC films for $t_h > 12 \text{ s}$ which can be explained by the fact that the model described by equation (3) does not take into account the opened channel structure and the contact of liquid to ambient air. Therefore, it is possible that a continuous flow of vaporized liquid electrolyte arises. Furthermore, with an increase in height of the capillary rise the hydrostatic pressure $\Delta\rho \cdot g \cdot h$ (equation 2) becomes more substantial and may be not neglected. Finally, the model also does not take into account the fact that a capillary flow perpendicular to the orientation of the channel structures may occur due to nano- and micro-porosity in NMC thick-film electrodes, lowering the liquid flow within the channel orientation.

Within an assembled lithium-ion pouch cell the channel structures are covered by the separator membrane and constant electrolyte evaporation may be neglected. Furthermore, the velocity of electrolyte penetration along nano-/micro-porosity is slow in comparison to the capillary flow velocity in direction of the laser generated channels. Therefore, by applying the boundary condition

$$\left. \frac{dh}{dt} \right|_{h=h_{\max}} = 0, \quad (4)$$

a maximum height of capillary rise can be calculated from equation 2:

$$h_{\max} = \frac{2\sigma_l \cos\theta}{r\rho g} \quad (5)$$

By applying the material properties for DMC and LP 30 (Table 2) to equation (5) as well as a capillary radius of $r \approx 23.5 \mu\text{m}$, a maximum height h_{\max} of 20 – 23 cm could be calculated. With respect to these calculations, electrolyte filling of lithium-ion pouch cells in a vertical arrangement as shown in Figure 2 would enable a maximum filling height of about 20 cm which is a theoretical limit. Nevertheless, this is a typical lateral dimension for a 40 Ah pouch cell.

Electrochemical cell tests

The internal electrical resistances of the cells were measured immediately after electrolyte filling and cell assembly as well as after 24 hours of cell storage at $T=22 \text{ }^\circ\text{C}$. Lithium-ion cells with unstructured NMC electrodes exhibited an electrical resistance of $(4.3 \pm 0.3) \cdot 10^6 \Omega$ while lithium-ion cells containing laser-structured NMC electrodes indicated an electrical resistance of $(0.260 \pm 0.005) \Omega$. It is assumed that this tremendous difference in electrical resistance directly after electrolyte filling and the cell assembly process is related to the difference in the amount of wetted NMC material for

unstructured and laser-structured electrodes. Furthermore, all lithium-ion cells exhibited electrical resistances in the range of 0.22Ω to 0.27Ω after 24 hours storage at room temperature indicating a homogenous electrolyte distribution within the electrodes (unstructured and laser-structured). The values for the internal electrical resistance are in the order of magnitude for data reported in literature.³⁹

Electrochemical cell performance after cell storage for 24 hours.

Galvanostatic testing was performed using a 1C rate (charge and discharge) for 1000 cycles (Figure 9).

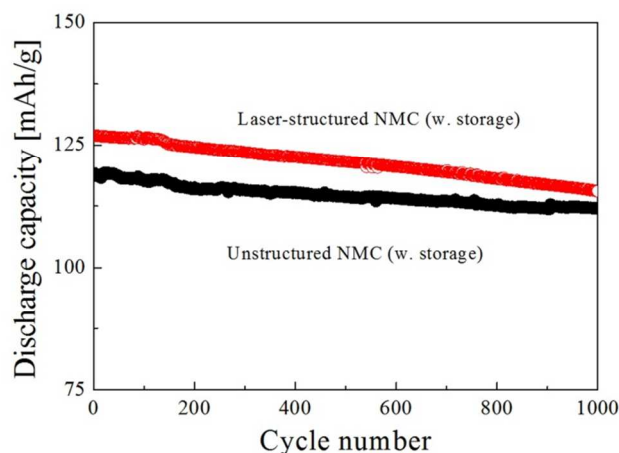


Figure 9: Specific discharge capacities of NMC pouch cells as function of cycle number (1 C charge/1 C discharge). Lithium-ion cells were stored for 24 hours prior to the cycling process (w. storage). Laser parameters for structuring: $P = 8.5 \text{ W}$, $v_{\text{rep}} = 80 \text{ kHz}$, $v = 200 \text{ mm/s}$, pitch distance $200 \mu\text{m}$.

For lithium-ion cells with unstructured and laser-structured NMC electrodes, the capacity retention after 1000 cycles differ slightly. During the first cycles at 1C discharge, the specific discharge capacity for lithium-ion cells with laser-structured NMC electrodes counts about 127 mAh/g while the discharge capacity for cells with unstructured NMC electrodes is about 119 mAh/g (Figure 9). After 1000 cycles the specific discharge capacity of cells with laser-structured and unstructured NMC thick-film electrodes decreases to 115 mAh/g and 112 mAh/g, respectively. The corresponding capacity retention is about $(92 \pm 2) \%$.

Electrochemical cell performance without cell storage for 24 hours.

By applying electrochemical cycling immediately after electrolyte filling and lithium-ion cell assembly, a tremendous difference in cycling behaviour between lithium-ion cells with unstructured and laser-structured NMC electrodes could be observed with respect to capacity retention and cell life-time (Figure 10). For cycle numbers up to $N=100$, the specific discharge capacity values are almost stable for both lithium-ion cells with unstructured and laser-structured NMC electrodes (see inset, Figure 10). For cycle number $N > 100$ lithium-ion

cells with unstructured NMC electrodes indicate a rapid decrease in discharge capacity (Figure 10).

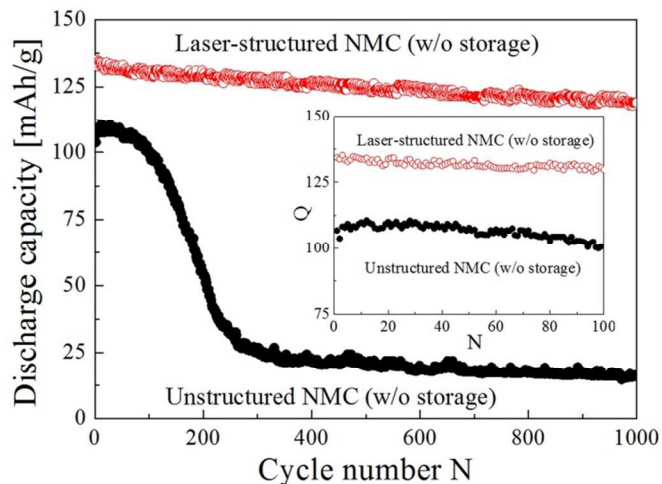


Figure 10: Specific discharge capacities of NMC pouch cells for cycle numbers up to $N=1000$ cycles (1 C charge/1 C discharge). Inset: capacity values for $N=100$ cycles. The cycling performance was investigated without cell storage after the assembly process. Laser parameters for structuring: $P = 8.5$ W, $\nu_{\text{rep}} = 80$ kHz, $v = 200$ mm/s, pitch distance $200 \mu\text{m}$.

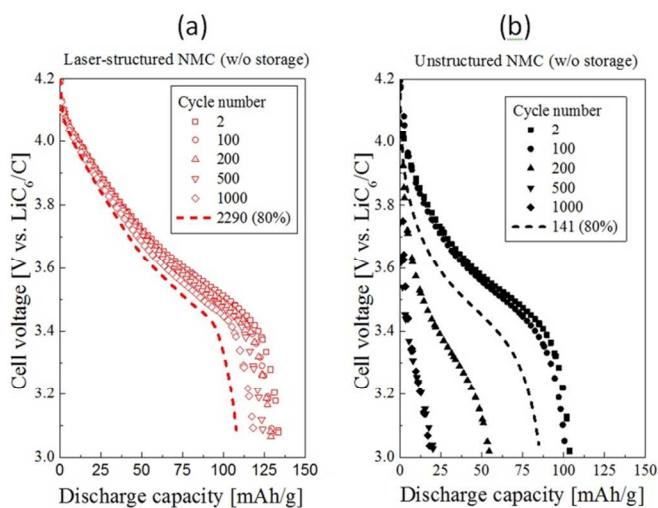


Figure 11: Cell voltage versus discharge capacity for laser-structured (a) and unstructured (b) NMC pouch cell cycled at 1 C charge/1 C discharge. The cycling performance was investigated without cell storage (w/o storage) after the assembly process. Laser parameters for structuring: $P = 8.5$ W, $\nu_{\text{rep}} = 80$ kHz, $v = 200$ mm/s, pitch distance $200 \mu\text{m}$.

A stable capacity retention was achieved for lithium-ion cells with laser-structured NMC cathodes (Figure 10). After 1000 cycles a specific discharge capacity of 120 mAh/g was measured for lithium-ion cells with laser-structured NMC films being quite close to the specific capacity of 116 mAh/g after 1000 cycles reached for lithium-ion cells with laser-structured NMC films and additional cell storage (w. storage) (Figure 9).

A characteristic capacity value for lithium-ion cells is the

80 % limit of the initial discharge capacity. When reaching 80 % of the initial discharge capacity, this is the so-called “cell life-time”. Capacity retention and cell life-time can be illustrated by plotting the cell voltage as function of discharge capacity for different cycle numbers. For the lithium-ion cell with the structured NMC electrode the 80 % capacity limit of the initial discharge capacity is reached after 2290 cycles (Figure 11a) while for the lithium-ion cell with unstructured electrodes the cell life-time is reached after 141 cycles (Figure 11b). Furthermore, the discharge capacity of the cell with the laser-structured NMC electrode reaches a value of 108 mAh/g after 2290 cycles which is very close to the initial capacity of 110 mAh/g of the cell with the unstructured NMC electrode.

Post-mortem studies were carried out in order to investigate the shape and surface of the laser structured NMC electrodes after cycling. Within these investigations, no film delamination or cracking of the microstructures could be observed. The shape of the structures remained intact and it was found that the surface of a structured electrode is very similar to the one of an unstructured electrode. It is obvious that the study of chemical modifications on the electrode surfaces (unstructured, structured) is quite challenging for composite films of porous nature and therefore, this work will be part of ongoing investigations.

Electrochemical tests with LMO electrodes.

Comparative studies with LMO electrodes were performed. It is shown that cell storage for 24 hours before electrochemical cycling of the cells leads to discharge capacities which are similar for both cells with and without laser-structured cathodes (Figure 12). The initial capacities for both types of cells are in the range of $(85 \pm 1) \text{ mAh/g}$. After 100 cycles specific capacities of 76 mAh/g and 70 mAh/g were achieved for cells with structured and unstructured electrodes, respectively. This corresponds to capacity retentions of 89 % and 82 %. Cells with structured electrodes show slightly improved cycling behaviour even after 24 hours cell storage. This may be due to the fact that the investigated LMO films with a thickness of $103 \mu\text{m}$ suffer even more from poor electrolyte penetration in comparison to unstructured material with decreased film thickness.

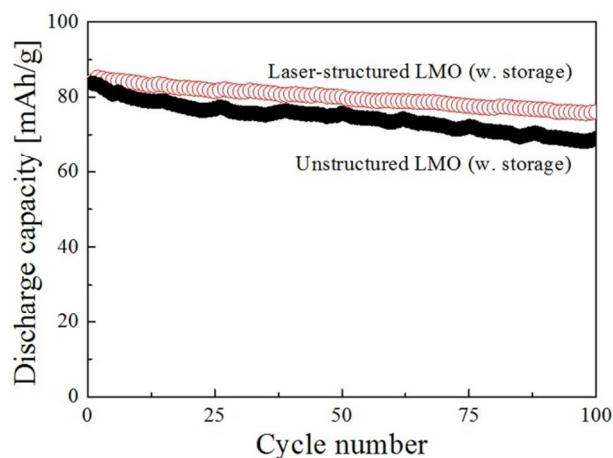


Figure 12: Specific discharge capacities of pouch cells with

laser-structured and unstructured LMO electrodes for 100 cycles (1 C charge/1 C discharge). Lithium-ion cells were stored for 24 hours prior to the cycling process (w. storage). Laser parameters for structuring: $P = 8.5$ W, $v_{\text{rep}} = 80$ kHz, $v = 200$ mm/s, pitch distance 200 μm .

The specific discharge capacity of cells with laser-structured and unstructured LMO electrodes was also investigated without cell storage (w/o storage) prior to electrochemical cycling (Figure 13).

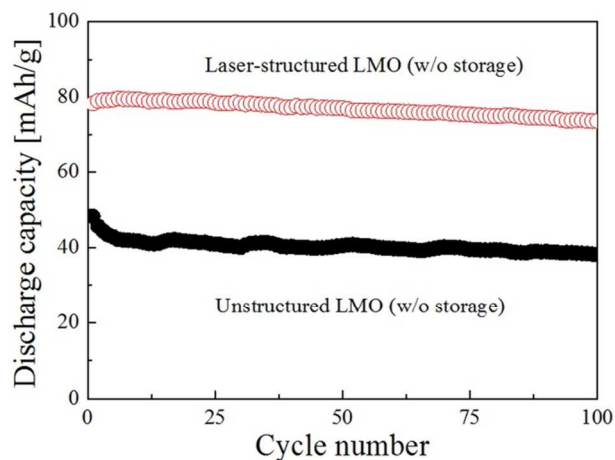


Figure 13: Specific discharge capacities of cells with laser-structured and unstructured LMO electrodes for 100 cycles (1 C charge/1 C discharge). The cycling performance was investigated without cell storage after the assembly process (w/o storage). Laser parameters for structuring: $P = 8.5$ W, $v_{\text{rep}} = 80$ kHz, $v = 200$ mm/s, pitch distance 200 μm .

Very similar to the obtained results with structured and unstructured NMC electrodes (Figure 10) a gap in initial specific discharge capacity between the cell with structured and the cell with unstructured cathode material was obtained. This is obviously due to insufficient electrolyte wetting of unstructured LMO electrodes. The cell with the structured LMO cathode exhibits an initial capacity of 80 mAh/g while the cell with the unstructured LMO electrode exhibits 48 mAh/g discharge capacity. After 100 cycles specific capacities of 74 mAh/g and 38 mAh/g could be measured for cells with structured and unstructured LMO electrodes, respectively. This corresponds to capacity retentions of 92% and 79% .

Within this comparative study it could be shown that an improvement in cycling stability and capacity retention could be achieved for both cells with laser-structured NMC and LMO electrodes. This improvement was assigned to enhanced electrolyte wetting of laser-structured NMC and LMO electrode materials. It is assumed that this type of electrode modification can be applied for each type of electrode material and/or composition where wetting with liquid electrolyte is a critical processing step in battery manufacturing.

Conclusions

In this paper we present a novel laser-based technique for dramatic acceleration of electrode wetting with liquid electrolyte. Laser-assisted structuring of tape cast cathode material was demonstrated to be an appropriate tool for forming micro-channels in the electrodes within the cell assembly process. It was shown that micro-channels with a width of about $40 - 55$ μm (NMC) and about 70 μm (LMO) and a maximum channel depth indicated the most appropriate wetting behaviour versus gravity as was described by the Washburn equation.

Electrochemical cell tests were performed using unstructured and laser-structured NMC or LMO cathodes. Within these studies it was demonstrated that lithium-ion cells consisting of an anode, separator membrane and a laser-structured cathode can be electrochemically primed immediately after electrolyte filling and cell assembly without additional storage condition. Acceleration and homogenization of electrolyte wetting both result in enhanced cell life-times and higher specific capacities. For unstructured NMC electrodes it was shown that inhomogeneous electrolyte wetting can lead to accelerated cell degradation and shortened cell life-times within the electrochemical cycling process.

Therefore, it is expected that higher flow-rates in production lines can be achieved due to the avoidance of time-consuming cell storage accompanied by less required storage capacities also leading to a reduction in failure production. Furthermore, safety issues are improved by using structured electrodes with the reduced risk of failure and occurrence of thermal runaway as it would be the case for incompletely wetted electrodes where inhomogeneous local current densities and hot-spots may promote cell degradation. With respect to high material costs in battery manufacturing, an electrode material mass loss of about 30 wt.% has to be further reduced by increasing the pitch in between two microstructures. A pitch of 600 μm would already push the of electrode material loss below 10 wt.%. The reduction of electrode material loss with respect to electrolyte wetting properties and electrochemical performance is currently under investigation.

In summary, it is assumed that the novel approach of using laser-generated capillary structures in the electrode materials can be applied in order to increase cell reliability during the production process, to shorten production times of lithium-ion cells as well as to increase the cell life-time during cycling. Furthermore, cost-efficient nanosecond fiber lasers can be applied for carrying out the structuring process. Ongoing research will focus on transferring the laser-structuring process to thick-film electrodes applicable for lithium-ion cells with capacities ranging from 5 Ah to 40 Ah.

Acknowledgements

We are grateful to our colleagues D. Przybylski and H. Besser for their technical assistance during laser material processing and cell assembly, N. Kandora for her technical assistance in SEM and D. Nötzel for her assistance during calendaring of

cathode materials. We gratefully acknowledge the financial support by the Helmholtz Association in frame of the "Helmholtz-Portfolio" about reliability and integration of battery systems. Finally, the support for laser processing by the Karlsruhe Nano Micro Facility (KNMF, <http://www.knmf.kit.edu>) a Helmholtz research infrastructure at the Karlsruhe Institute of Technology is gratefully acknowledged.

References

1. J. B. Goodenough and Y. Kim, *Chem. Mater.*, 2010, **22**, 587-603.
2. B. Scrosati and J. Garche, *J. Power Sources*, 2010, **195**, 2419-2430.
3. J. W. Long, B. Dunn, D. R. Rolison and H. S. White, *Chem Rev*, 2004, **104**, 4463-4492.
4. R. Kohler, H. Besser, M. Hagen, J. Ye, C. Ziebert, S. Ulrich, J. Proell and W. Pfleging, *Microsyst Technol*, 2011, **17**, 225-232.
5. P. H. L. Notten, F. Roozeboom, R. A. H. Niessen and L. Baggetto, *Adv. Mater.*, 2007, **19**, 4564-4567.
6. J. F. M. Oudenhoven, L. Baggetto and P. H. L. Notten, *Adv. Energy Mater.*, 2011, **1**, 10-33.
7. A. V. Jeyaseelan and J. F. Rohan, *Appl. Surf. Sci.*, 2009, **256**, 61-64.
8. H. Kim, R. C. Y. Auyeung and A. Piqué, *J. Power Sources*, 2007, **165**, 413-419.
9. C. L. Wang, L. Taherabadi, G. Y. Jia, M. Madou, Y. T. Yeh and B. Dunn, *Electrochem. Solid State Lett.*, 2004, **7**, A435-A438.
10. B. Dunn, C. J. Kim and S. Tolbert, in *Proceedings of the IEEE International Conference on Micro Electro Mechanical Systems (MEMS)*, eds. M. Wong and Y. Suzuki, IEEE, New York, 2010, pp. 164-167.
11. W. C. West, J. F. Whitacre, V. White and B. V. Ratnakumar, *J. Micromech. Microeng.*, 2002, **12**, 58-62.
12. L. Baggetto, R. A. H. Niessen, F. Roozeboom and P. H. L. Notten, *Adv Funct Mater*, 2008, **18**, 1057-1066.
13. B. Ketterer, H. Vasilchina, K. Seemann, S. Ulrich, H. Besser, W. Pfleging, T. Kaiser and C. Adelhelm, *Int. J. Mater. Res.*, 2008, **99**, 1171-1176.
14. J. Pröll, R. Kohler, C. Adelhelm, M. Bruns, M. Torge, S. Heissler, M. Przybylski, C. Ziebert and W. Pfleging, *Proc Spie*, 2011, **7921**, Q01-Q14.
15. R. Kohler, P. Smyrek, S. Ulrich, M. Bruns, V. Trouillet and W. Pfleging, *J. Optoelectron. Adv. Mater.*, 2010, **12**, 547-552.
16. R. Kohler, J. Proell, S. Ulrich, V. Trouillet, S. Indris, M. Przybylski and W. Pfleging, *Proc Spie*, 2009, **7202**, 0701-0711.
17. R. Kohler, M. Bruns, P. Smyrek, S. Ulrich, M. Przybylski and W. Pfleging, *Proc Spie*, 2010, **7585**, O01-O11.
18. J. Proell, R. Kohler, M. Torge, S. Ulrich, C. Ziebert, M. Bruns, H. J. Seifert and W. Pfleging, *Appl. Surf. Sci.*, 2011, **257**, 9968-9976.
19. J. Pröll, R. Kohler, A. Mangang, S. Ulrich, M. Bruns, H. J. Seifert and W. Pfleging, *Appl. Surf. Sci.*, 2012, **258**, 5146-5152.
20. J. H. Park, R. Kohler, W. Pfleging, W. Choi, H. J. Seifert and J. K. Lee, *RSC Adv.*, 2014, **4**, 4247-4252.
21. D. G. Lim, D.-W. Chung, R. Kohler, J. Proell, C. Scherr, W. Pfleging and R. E. García, *J. Electrochem. Soc.*, 2014, **161**, A302-A307.
22. R. Kohler, J. Proell, M. Bruns, S. Ulrich, H. J. Seifert and W. Pfleging, *Appl. Phys. A*, 2013, **112**, 77-85.
23. H. Kim, J. Proell, R. Kohler, W. Pfleging and A. Pique, *J. Laser Micro Nanoen.*, 2012, **7**, 320-325.
24. J. Pröll, H. Kim, A. Piqué, H. J. Seifert and W. Pfleging, *J. Power Sources*, 2014, **255**, 116-124.
25. A. Jossen, J. Garche and D. U. Sauer, *Sol Energy*, 2003, **76**, 759-769.
26. G. Amatucci, A. Du Pasquier, A. Blyr, T. Zheng and J. M. Tarascon, *Electrochim Acta*, 1999, **45**, 255-271.
27. H. S. Jeong, E. S. Choi, S. Y. Lee and J. H. Kim, *J Membrane Sci*, 2012, **415**, 513-519.
28. J. Choi, E. Morikawa, S. Ducharme and P. A. Dowben, *Mater Lett*, 2005, **59**, 3599-3603.
29. A. Slocombe and L. Li, *Appl. Surf. Sci.*, 2000, **154**, 617-621.
30. M. F. Jensen, M. Noerholm, L. H. Christensen and O. Geschke, *Lab Chip*, 2003, **3**, 302-307.
31. W. Pfleging and O. Baldus, *Proc Spie*, 2006, **6107**, 7501-7512.
32. E. W. Washburn, *Phys. Rev.*, 1921, **17**, 273-283.
33. A. Lundblad and B. Bergman, *J. Electrochem. Soc.*, 1997, **144**, 984-987.
34. M. S. Wu, T. L. Liao, Y. Y. Wang and C. C. Wan, *J. Appl. Electrochem.*, 2004, **34**, 797-805.
35. F. Wang, J. Wu and Z. Liu, *Fluid Phase Equilib.*, 2004, **220**, 123-126.
36. M. Dahbi, D. Violleau, F. Ghamouss, J. Jacquemin, T. V. Francois, D. Lemordant and M. Anouti, *Ind Eng Chem Res*, 2012, **51**, 5240-5245.
37. M. Morita, Y. Asai, N. Yoshimoto and M. Ishikawa, *J Chem Soc Faraday T*, 1998, **94**, 3451-3456.
38. K. Kwon and J. Evans, *Electrochemical and Solid-State Letters*, 2002, **5**, A59-A61.
39. L. Gao, S. Liu and R. A. Dougal, *IEEE Trans. Compon. Packag. Technol.*, 2002, **25**, 495-505.